Effect of a pre-oxidation on the hydrogen desorption from Zircaloy-4

Clara Juillet, Marc Tupin, Frantz Martin, Quentin Auzoux, Sophie Bosonnet, Clément Berthinier

Effect of a pre-oxidation on the hydrogen desorption from Zircaloy-4

C. Juillet[(1)], M. Tupin[(2)], F. Martin[(1)], Q. Auzoux[(1)], S. Bosonnet[(1)], C. Berthinier[(3)]

(1) Den-Service de la Corrosion et du Comportement des Matériaux dans leur Environnement (SCCME), CEA, Université Paris-Saclay, F-91191, Gif-sur-Yvette, FRANCE
(2) Den-Service d'Etude des Matériaux Irradiés (SEMI), CEA, Université Paris-Saclay, F-91191, Gif-sur-Yvette, France
(3) Den-Service d'Etude Mécaniques et Thermiques (SEMT), CEA, Université Paris-Saclay, F-91191, Gif-sur-Yvette, France

Corresponding author: clara.juillet@cea.fr (C. Juillet)

1   Abstract

During the transport of nuclear spent fuel, part of the tritium formed by ternary fission in core of nuclear reactors is susceptible to desorb from the oxidized cladding. This study aimed at identifying the rate-limiting step in the hydrogen desorption process from pre-oxidized Zircaloy-4 specimens. Controlled-thickness oxide scales shifted the hydrogen desorption from the alloy towards higher temperatures during a temperature ramp under vacuum. Scanning electron microscopy observations and finite elements modelling of the oxide layer dissolution led to the conclusion that, in such conditions, hydrogen desorption from the alloy was controlled by the oxide dissolution kinetics.

2   Introduction

Under normal operating conditions in nuclear pressurized water reactors (PWRs), the external surface of zirconium alloy fuel cladding is exposed to primary water and continuously oxidized, process during which the cladding absorbs a fraction of the hydrogen produced by water reduction. In the fuel rod, ternary fission occurring within the uranium oxide fuel leads to the formation of

1

tritium. The inner surface of the cladding is also oxidized by initial residual water and by the uranium oxide [1]. During the transport of spent fuel, part of this hydrogen and tritium may desorb from the cladding, which implies safety concerns. A closer understanding of the associated hydrogen species transport phenomena, especially the influence of an oxide layer on the tritium desorption from the cladding, is a keystone for a better estimation of potential tritium release. The aim of the present study, in the long term, is to identify and quantify the rate-limiting step in the desorption process of hydrogenated species from usual cladding materials such as Zircaloy-4 (referred to as Zy4 thereafter). A first study was realized on an unoxidized Zy4 sheet, a less complex system [2]. We demonstrated that hydrogen desorption kinetics from the metal was limited by its molecular recombination reaction on the surface. It was then decided to study a more realistic system: the present work focuses on the influence of a pre-oxidation on hydrogen desorption from a Zy4 sheet. Pre-oxidations were performed in a thermogravimetric device in dry oxygen atmosphere to prevent hydrogen absorption during oxidation. The only source of hydrogen considered here was internal hydrogen, coming from the material elaboration process.

The hydrogen release from the bulk alloy can be decomposed into five elementary steps, inspired by literature-suggested physicochemical steps [3,4]:

1. Hydrogen diffusion through the alloy towards the metal/oxide interface, generally via interstitial sites [5];

2. Integration into the oxide lattice (or into the grain boundaries of the oxide) by crossing the metal/oxide interface;

3. Diffusion through the oxide towards the subsurface;

4. Passing from subsurface sites to surface sites as adsorbed species;

5. Final recombination into dihydrogen molecules and desorption from the oxide surface.

The hydrogen diffusion process through the α-Zr matrix has been widely investigated in the past leading to a thorough estimation of the hydrogen diffusion coefficient in the zirconium alloys [6–13]. Average diffusion coefficient of hydrogen through the α-Zr matrix deduced from the references [6–13] is basically expressed as follows (1),

$$D_{H\_Zr} = D^0_{H\_Zr} \cdot exp\left(-\frac{E_a}{RT}\right) = 10^{-7} \cdot exp\left(-\frac{35000}{RT}\right) \quad (m^2 \, s^{-1}) \tag{1}$$

where $D^0_{H,Zr}$ englobes diffusion entropy change and jump probability, E_a corresponds to the migration enthalpy (in J mol^{-1}), T is the temperature (in K) and R the ideal gaz constant (8.314 J K^{-1} mol^{-1}).

Taking into account expression (1), our previous study [2] showed that the process of hydrogen desorption from a sheet of unoxidized Zy4 alloy, occurring in the 773 − 1073 K temperature range, was not rate-limited by the hydrogen diffusion step through the alloy.

Hydrogen diffusion mechanism in the oxide layer is widely discussed in the literature but the measured values of hydrogen diffusion coefficients are very scattered and dependent on the experimental procedures, the analysis techniques and the sources of hydrogen (absorption by water corrosion process, implantation, gaseous charging into the alloy …) that were used. This coefficient basically varies by many orders of magnitude, for example between 10^{-17} and 10^{-14} cm^2 s^{-1} at 573 K [13–16]. In any case, the apparent hydrogen diffusion rate through the oxide scale is much lower than in the alloy.

Several authors observed a decrease of the hydrogen release rate due to the presence of an oxide layer on the surface [8,14,16–21]. Chen [18], Wongsawaeng [20] and Roustila [21] were interested in the hydrogen desorption from oxidized hydrides. Chen et al. [18] demonstrated, by comparing hydrogen thermal desorption spectra (TDS) obtained on zirconium hydrides in two atmospheres (He and He-5%O_2), that an oxide layer composed of monoclinic ZrO_2 and small amount of tetragonal $ZrO_{1.88}$ acted as a very effective diffusion barrier. Andrieu [17,22], who was interested in tritium permeation through Zy4 in primary water, concluded that the tritium permeation rate-limiting step was the tritium transport through the oxide layer for experiences carried out at 619 K during 252 days.

In addition, Andrieu [17,22] observed an oxide scale dissolution into the alloy during a temperature ramp or a long isothermal treatment. This dissolution is due to the difference of oxygen chemical potential between the oxide and the metal and is enhanced by the high solubility of oxygen in zirconium [23]. For example at 1123 K, the atomic percentage of oxygen can reach 30%, and 29% around 670-770 K [24]. The concentration of dissolved oxygen in the alloy beneath the oxide layer is thus around a few tens percent.

Greger [8] and Kunz [19] investigated the influence of dissolved oxygen on the tritium diffusion in Zircaloy-2. They did not observe any significant deviation of the tritium diffusion coefficient in Zircaloy-2 for oxygen concentrations ranging between 1000 and 11300 wt.ppm [8] and up to 10 at.% of dissolved oxygen [19].

Based on available literature data mentioned above, it seems now obvious that diffusion in the alloy itself, containing oxygen or not, may clearly not be the rate limiting step in the desorption process of hydrogen from an oxide-covered Zy4. Nevertheless, among the five potential rate-limiting steps enumerated earlier, the four last points are still possible candidates and need to be investigated.

In the present study, the hydrogen desorption process through an oxide layer was studied during temperature ramps under vacuum, following the same approach of Hirohata on TA6V alloy [25]. The

aim was to determine the rate-limiting step of the hydrogen desorption kinetics from an oxidized Zy4 specimen. To reach this goal, a thermogravimetric analysis device was used to carry out oxidation in dry atmosphere (Ar-20%O_2), then the hydrogen desorption rate was quantified by TDS technique [2,26,27]. The oxide scale dissolution during TDS temperature ramp was computed using Cast3M, the finite elements (FE) code developed at CEA [28,29]. The oxide dissolution state was investigated by Scanning Electron Microscopy (SEM) analysis and via FE simulations, which results were compared with TDS hydrogen desorption temperatures.

3 Experimental Procedure

3.1 Material and specimen preparation

A 0.45-mm thick sheet of recrystallized Zy4 alloy supplied by FRAMATOME^{TM} was used. The chemical composition of the alloy is given in Table 1. Rectangular specimens (1 x 1.5 cm) were cut from the sheet to get one side surface area of around 1.5 cm². The surfaces were ground with SiC emery paper up to grade P2000. Additional final polishing was done with ¼ µm diamond paste. The final thickness of the sample was around 350 µm (0.35 mm).

Table 1. Chemical composition of the Zircaloy-4 alloy.

Alloying elements	Fe (wt.%)	Cr (wt.%)	Sn (wt.%)	O (wt.%)	C wt.ppm	H wt. ppm	Zr
Zircaloy-4	0.19 – 0.21	0.11	1.31 – 1.35	0.11 – 0.12	118 – 129	20 – 30	Bal.

3.2 SEM characterization

The characterization of the samples was carried out with an Ultra 55 Zeiss™ Field Emission Gun SEM using the secondary electrons detector. To prevent oxide scale degradation during preparation of the cross-sections, a gold deposition was first performed with a Quorum Q 150 R ES metallizer (with a current intensity of 40 mA during 1 min) on specimens. Afterwards, the samples were electrochemically nickel-coated using a Watts bath at 323 K with a cathodic current intensity equal to 10 mA during 5 min followed by 10 min at 100 mA.

3.3 Thermogravimetric analysis

Oxidation was performed in a symmetrical microbalance Setaram™ TGA 16 apparatus (with a 10^{-6} g accuracy and a flow rate inside each furnace of 1.25 L h^{-1}). Thermal cycle is composed of heating ramp at 50 K min^{-1}, a dwell at the target temperature (623 K, 673 K and 773 K), the duration of the dwell depending on target oxide thickness and thus the measured weight gain during experiment. Heating was under He atmosphere to limit significant oxidation. Oxidation was performed under argon containing 20% O_2, introduced at the beginning of the thermal dwell.

The TGA apparatus made it possible to accurately follow the oxide thickness evolution by monitoring the sample's weight gain using the CALISTO® software.

3.4   Thermal Desorption Spectrometry

The kinetics of hydrogen desorption was determined by thermal desorption analyses. The thermal desorption spectrometry set-up developed at the CEA used in this study was made of a quartz tube under vacuum (10^{-6} – 10^{-7} mbar) surrounded by a cylindrical furnace coupled to a quadrupole mass spectrometer (Transpector 100-M INFICON™). By imposing an external temperature ramp (by means of the tubular furnace), the specimen was heated up, desorbed species were then ionized, separated, detected and counted by the mass spectrometer. Hydrogen species could therefore be detected and eventually quantified thanks to the deuterium ($^2H_2$) calibration previously done. The investigated temperature ranged between 298 K and 1273 K. Data were processed by TWare32® or FabGuard® Explorer software.

4   Results and discussion

4.1   Oxidation kinetics

In order to study the influence of the oxide layer on the hydrogen desorption process, Zy4 sheets were oxidized up to final oxide thicknesses varying in the 30 nm - 630 nm range.

For the lowest oxide thickness (some tens nanometers), thermogravimetric analysis in Ar-20%O_2 atmosphere was performed at low temperature, at 623 K, while other specimens were oxidized at 673 and 773 K to reach 300-nm and 630-nm thick oxide layers, respectively. The different temperatures were chosen to form the desired oxide thickness in reasonable time scales and

minimize desorption of elaboration hydrogen from the alloy during this step. It was indeed shown in [2] that below 800 K on bare Zy4, no (or very few) hydrogen desorption occurred.

The mass variation with exposure time obtained in these conditions is shown in Figure 1.
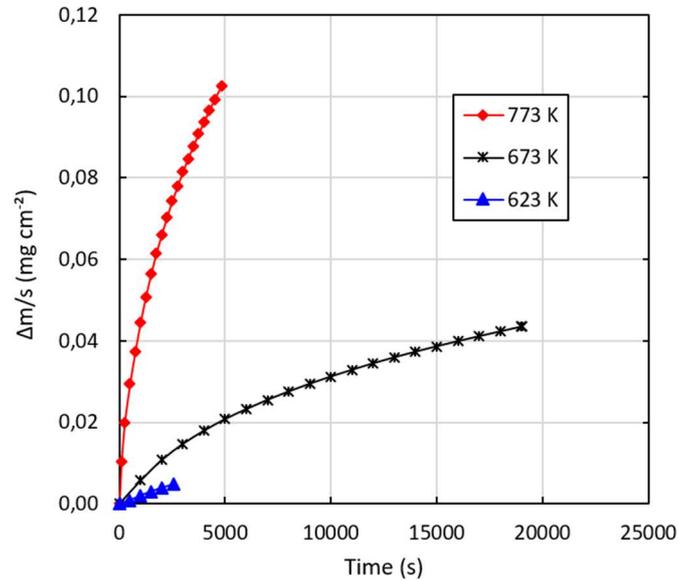

Fig. 1. Specific mass variation of Zy4 specimens with oxidation time in Ar-20%O_2 at: 773 K (red curve), 673 K (black curve) and 623 K (blue curve).

For temperatures lower than 823 K, the oxide thickness (X in cm) can be deduced from the weight gain according to the following formula (2) [30] :

$$X = \frac{M_{ZrO2}}{\rho_{ZrO2}} \frac{\Delta m/_S}{M_{O2}} \tag{2}$$

where M_{ZrO2} and M_{O2} are the molar masses of zirconia (123.2 g mol^{-1}) and dioxygen gas (32 g mol^{-1}) respectively, ρ_{ZrO2} the density of zirconia (5.68 g cm^{-3}) and $\Delta m/_S$ the mass variation per unit area (g cm^{-2}). The ratio $\frac{M_{ZrO2}}{\rho_{ZrO2}}$ corresponds actually to the molar volume, V_e, of zirconia (cm^3 mol^{-1}).

Since the target, oxide thicknesses were relatively low compared to what is generally achieved in high temperature oxidation studies, the reliability of the measurements was tested with respect with oxide growth kinetics and compared with literature data. Such validation would allow the use of rapid calculations for the dimensioning of the oxidation experiments to reach the desired oxide thicknesses in terms of temperature and duration under Ar-20%O_2 atmosphere.

 To this aim, experimental data were fitted using the kinetics law (3) for a mixed regime (diffusion - interface reaction) suggested by Evans [31]:

$$\frac{de}{dt} = \frac{1}{\left(\frac{1}{k_l}+\frac{2e}{k_p}\right)} = \frac{k_p/2}{\left(\frac{k_p}{2k_l}+e\right)} \tag{3}$$

with k_p the parabolic rate constant for a diffusion rate limiting step (RLS), k_l the rate constant for an interface reaction RLS and e the oxide thickness.

This law can be deduced from the so-called theorem of "the equality of rates" for a mixed regime [32]. This theorem states that the inverse of the oxidation rate for a mixed regime of interface reaction and diffusion step is the sum of the inverses of the rate of each pure regime (interface reaction and diffusion) considered separately. Assuming that vacancy diffusion process through the oxide layer formed on Zy4 alloy is the rate limiting step as shown in reference [30], the parabolic rate constant is given by the following formula (4):

$$k_p = 2V_e D_v C_v = 2V_e D_v x_v C_o = 4D_v x_v \tag{4}$$

where V_e is the molar volume of zirconia (21.7 cm^3 mol^{-1}), D_v the vacancy diffusion coefficient, C_v and C_o the vacancy and oxygen concentrations at the metal/oxide interface, respectively (mol cm^{-3}) and x_v the molar fraction of oxygen vacancies (compared to anionic sub-lattice).

For a vacancy diffusion mechanism, the vacancy diffusion coefficient is linked to the oxygen diffusion one according to the following equation (5):

$$D_o x_o \cong D_o = D_v x_v \tag{5}$$

with D_o the oxygen diffusion coefficient and x_o the molar fraction of oxygen ions (compared to anionic sub-lattice *i.e.* x_O is equal to 1-x_v), which is close to one in weakly sub-stoichiometric zirconia. The parabolic constant is thus expressed as follows (6):

$$k_p = 4D_v x_v = 4D_o \tag{6}$$

and equation (3) becomes (7):

$$\frac{de}{dt} = \frac{2D_o}{\left(\frac{2D_o}{k_l}+e\right)} \tag{7}$$

The oxidation kinetics at 673 and 773 K *i. e.* for the highest final oxide thicknesses were fitted with the law described by (7) in order to extract two parameters for each temperature: D_o and $\frac{2D_o}{k_l}$.

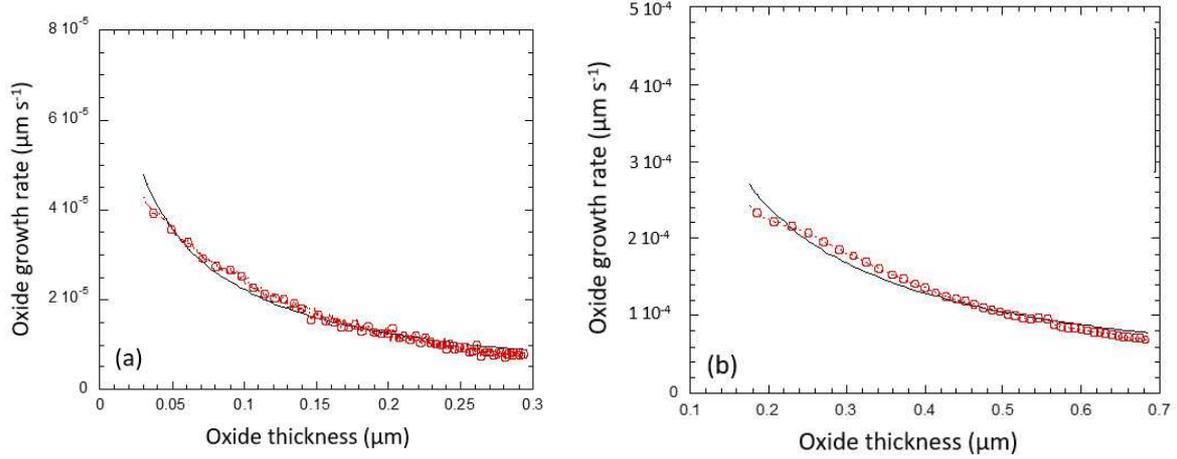Figure 2 shows the fitted curves compared with experimental data.

Fig. 2. Oxide growth rate versus oxide thickness deduced from the measured mass variations at: (a) 673K and (b) 773 K. The black continuous curve corresponds to the fit of the experimental data (red empty dots) with (Eq. (7)) and Do and (2Do/kl) values gathered in Table 2.

Table 2 sums up the values of the fitted parameters and the oxygen diffusion coefficient as well as the interface reaction rate constant.

Table 2. Values of the fitted parameters and oxygen diffusion coefficient at 673 and 773 K.

T(K)	D_o ($\mu m^2 s^{-1}$)	$2D_o/k_l$ (μm)	k_l (cm s^{-1})	D_o (cm^2 s^{-1})
673	1.44x10^{-6}	3.00x10^{-2}	9.60x10^{-9}	**1.44x10^{-14}**
773	2.80x10^{-5}	3.28x10^{-2}	1.71x10^{-7}	**2.80x10^{-13}**

The migration energy of oxygen was estimated from the oxygen diffusion coefficient ratio between these two temperatures according to the following formula (8), assuming an Arrhenius–type behaviour:

$$E_m = -R \left(\frac{1}{\frac{1}{T_2} - \frac{1}{T_1}} \right) \ln \left(\frac{D_o(T_2 = 773K)}{D_o(T_1 = 673K)} \right) \rightarrow \quad E_m = 128 \text{ kJ mol}^{-1} \qquad (8)$$

Then the pre-exponential factor was deduced according to equation (9):

$$D_o^0 = \frac{D_o(T_2 = 773K)}{\exp\left(-\frac{E_m}{R(T_2)}\right)} \quad \rightarrow \quad D_o^0 = 1.32\text{x}10^{-4} \text{ cm}^2 \text{ s}^{-1} \qquad (9)$$

The migration energy found is similar to the values mentioned in literature, in particular in Parise's work (~ 131 kJ mol^{-1}) [33] or those of references [34–36]. The pre-exponential factor is also consistent with the value given in Parise's thesis (~ 6.8x 10^{-4} cm^2 s^{-1}).

It is worth noting that the interface reaction rate constant is ten times higher than the ratio $2D_o/X$ for X > 0.3 µm, meaning that beyond around 0.3 µm oxide thicknesses, the rate limiting step is the oxygen diffusion process only.

In brief, the oxidation kinetics measured by thermogravimetric analysis on Zy4 alloy and the kinetic parameters such as migration energy of oxygen in the oxide layer are consistent with literature data. This brief analysis validates the procedure adopted in the present work to obtain a controlled oxide thickness.

4.2   Thermal desorption spectrometry experiments

The Thermal Desorption Spectrometry (TDS) technique was used to study the hydrogen desorption kinetics. Figure 3 compares the hydrogen desorption flux obtained on various pre-oxidized Zircaloy-4 samples. These TDS experiments were carried out following a 10 K min^{-1} temperature ramp from 293 K up to 1273 K.
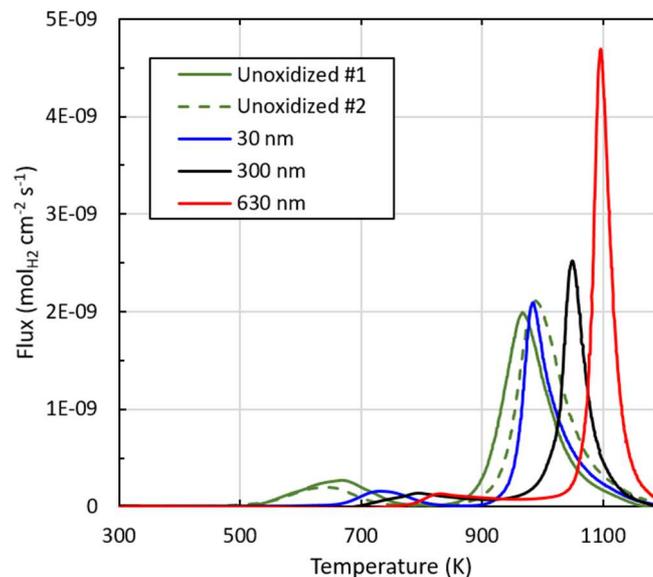

Fig. 3. Experimental TDS H$_2$ desorption flux obtained during 10 K min^{-1} temperature ramps on unoxidized Zy4 samples (green and green dashed curve) and pre-oxidized Zy4 samples with different initial zirconia thicknesses: 30 nm (blue curve), 300 nm (black curve) and 630 nm (red curve).

Figure 3 shows two hydrogen desorption peaks regardless of the oxide layer thickness on the surface sample. As discussed in our previous article [2], the first hydrogen desorption peak is representative of hydrogen release during the reduction on the sample of the residual water vapour present in the quartz device. Independently of the sample pre-oxidation, the oxide thickness formed during the TDS

9

experiment is approximately 40 $\pm$ 5 nm [2]. Note that the initial oxide thicknesses become, after this first peak during the TDS temperature ramp, 70, 340 and 670 nm (referring to initial thicknesses of 30, 300 and 630 nm respectively). Only the second hydrogen desorption peak being representative of hydrogen desorption from the metal, particular attention was paid to this second peak. The amount of hydrogen desorbed from the specimens during the TDS experiment was estimated by integration of the flux as function of time, only during the second hydrogen desorption peak. For every sample, the amount found was about 20 wt. ppm, which corresponds well to the initial hydrogen concentration measured by total melting extraction method on samples extracted from the same sheet (25 $\pm$ 5 wt. ppm). Figure 3 reveals a shift of hydrogen desorption peaks towards higher temperatures while increasing the oxide thickness. In agreement with literature [8,14,16–20], these results show a strong barrier effect of the oxide layer on the hydrogen desorption process. Besides, as observed in Andrieu's work [17,22] and in our previous work [2], the oxide scale may partially dissolve into the alloy during the temperature ramp. The question arising here is as follows: what was the extent of the dissolution of the oxide scale when the hydrogen desorption occurred? In case of a negligible oxide dissolution, the increasing peak shift could be interpreted as resulting from the diffusion through a thicker oxide; in case of an important oxide dissolution, the increasing peak shift could be interpreted as resulting from the longer time needed for a thicker oxide to dissolve into the metal, then reducing the barrier to hydrogen desorption.

In our previous work on the hydrogen desorption from a Zircaloy-4 alloy [2], X-ray photoelectron spectroscopy analysis demonstrated the native oxide dissolution before hydrogen desorption (at around 873 K). This result shows the significant role of the oxide layer dissolution on the hydrogen desorption kinetics. The next paragraphs are therefore dedicated to the study of this dissolution process during the TDS experiments.

4.3   Oxide scale dissolution

4.3.1   SEM cross-section characterisation after interrupted TDS experiments

Complementary TDS experiments were carried out on specimens having the three oxide aforementioned thicknesses and were interrupted before the metal-corresponding hydrogen desorption peak, *i.e.* at   873 K for 70 nm-thick oxide specimen, 900 K for 340 nm-thick oxide specimen and 950 K for 670 nm-thick oxide specimen. The oxide layer morphologies were observed by SEM on cross-section at 5 – 10 kV voltage. Figure 4 (70 nm), Figure 5 (340 nm) and Figure 6 (670 nm) display the various full and interrupted TDS experiments and the respective SEM cross-sections.
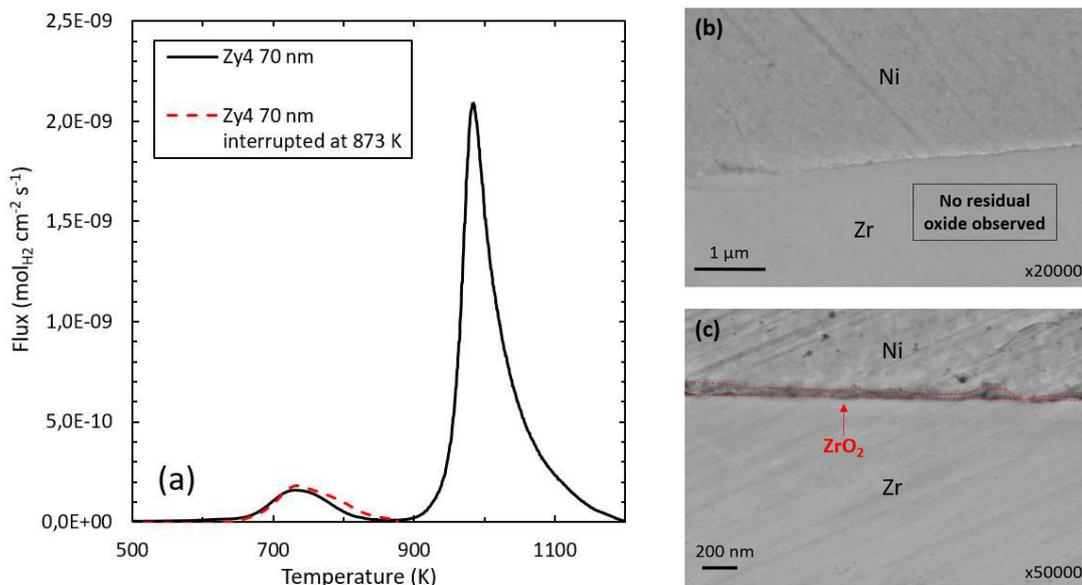
Fig. 4. (a) Experimental TDS H$_2$ desorption fluxes obtained on oxidized Zy4 samples with 70 nm-thick oxide layer during 10 K min^{-1} temperature ramps (the experiment interrupted at 873 K figures in dashed line). (b) and (c) SEM (secondary electrons) cross-section morphologies of the associated pre-oxidized Zy4 after the 873 K-interrupted TDS experiment.

Fig. 5. (a) Experimental TDS H$_2$ desorption fluxes obtained on oxidized Zy4 samples with 340 nm-thick oxide layer during 10 K min^{-1} temperature ramps (the experiment that was interrupted at 900 K is shown in dashed line). (b) and (c) SEM (secondary electrons) cross-section morphologies of the associated pre-oxidized Zy4 after the 900 K-interrupted TDS experiment.
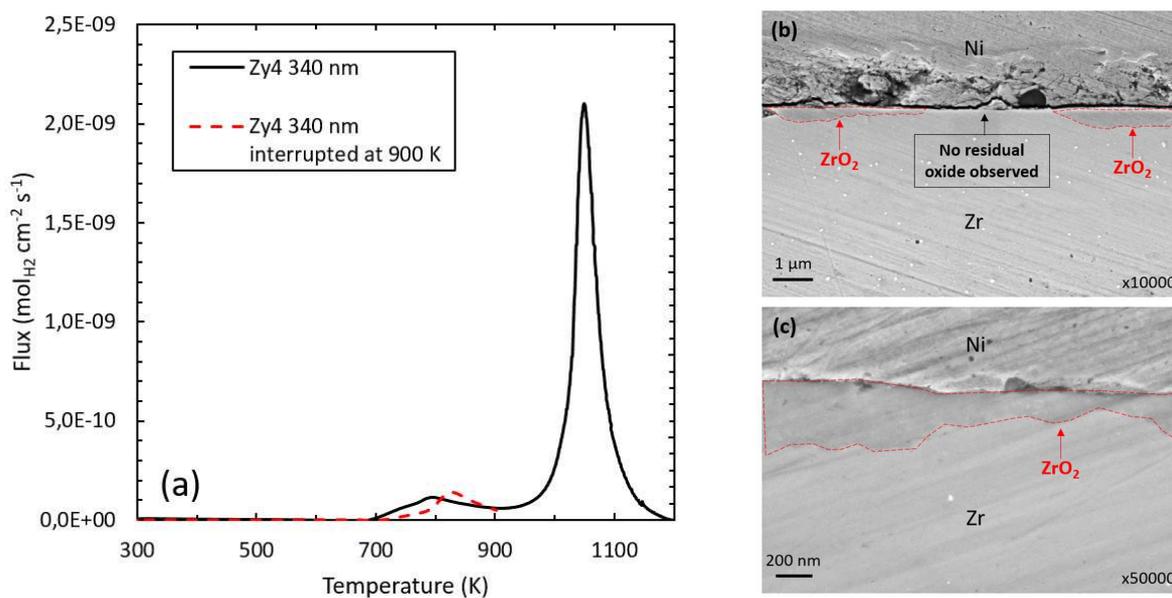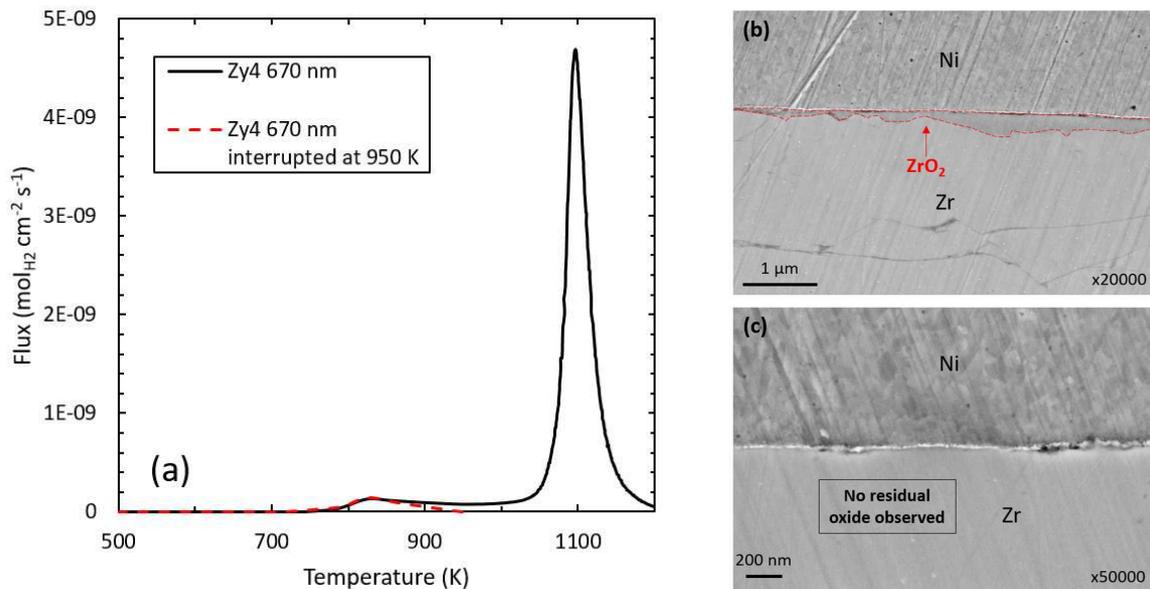
Fig. 6. (a) Experimental TDS H_2 desorption fluxes obtained on oxidized Zy4 samples with 670 nm-thick oxide layer during 10 K min^{-1} temperature ramps (the experiment that was interrupted at 950 K is shown in dashed line). (b) and (c) SEM (secondary electrons) cross-section morphologies of Zy4 oxidized after the 950 K-interrupted TDS experiment.

Independently of the initial oxide thickness present on the specimens, Figures 4, 5 and 6 show a heterogeneous oxide layer dissolution. It appears indeed that the oxide layer is still present in some areas while it seems to have completely disappeared from the surface of the metal elsewhere (SEM observation limit of around 10 nm). The areas without oxide observable by SEM will likely provide preferential paths for hydrogen desorption at the beginning of the release process. In order to obtain more insights into the dissolution kinetics of the oxide scale into the Zy4 alloy during the actual experimental temperature ramp, finite elements calculations were performed. They are described in the next section.

4.3.2   Simulation of the oxide scale dissolution

The dissolution of the oxide layer was studied following the same methodology as in our previous article [2]. The objective here is to estimate the temperature corresponding to the complete dissolution of the oxide layer and to compare simulation results with TDS experiments.

The dissolution process during the temperature ramp was numerically solved by finite elements (FE) using the Cast3M code [28,29]. To solve this complex moving boundaries problem, two major simplifications were made: (i) the oxide layer was considered as an unlimited source of oxygen and (ii) the oxygen concentration in the alloy at the metal/oxide interface was assumed to be constant

12

and equal to 30 at.%, which corresponds to the saturation concentration of oxygen in the α-Zr matrix (boundary condition).

The diffusion equation used in the Cast3M code was Fick's second law (10):

$$\frac{\partial C_{O\_Zr}}{\partial t} = \vec{\nabla} \cdot \left(D_{O\_Zr} \overrightarrow{\nabla(C_{O\_Zr})} \right) \tag{10}$$

The oxygen diffusion coefficient in Zircaloy-4 alloy, extensively studied in literature [23], can be expressed as follows (11) [33]:

$$D_{O\_Zr} \cong 6 \ 10^{-5} . \exp\left(-\frac{197237}{RT}\right) \qquad (m^2 \ s^{-1}) \tag{11}$$

where T is the temperature (in K) and R the ideal gas constant (8.314 J K^{-1} mol^{-1}).

The effective available oxygen amount per unit area, for each oxide thickness, was quantified as follows: (i) the total amount of oxygen per unit area in the oxide, n_{O_ZrO2}, was calculated, (ii) among these oxygen atoms, some were assumed unavailable for diffusion in the alloy since they will finally be part of the newly formed "oxygen –saturated alloy" in place of the former oxide layer, representing 30 at.% of oxygen in this "new" matrix, giving the "immobile" oxygen atoms amount per unit area n_{O_Zr}, and (iii) the difference between these two quantities gave the amount of oxygen atoms per unit area n_{O_mobile} involved in the diffusion process in the alloy corresponding to oxide dissolution.

For each initial oxide thickness, this "mobile oxygen" amount per unit area n_{O_mobile} was calculated thanks to following equations (12-14):

$$n_{O\_ZrO2} = 2 \times e_{ZrO_2} \times 10^{-9} \times \frac{\rho_{ZrO2}}{M_{ZrO2}} \times 10^6 \tag{12}$$

with e_{ZrO2} the oxide thickness in nm, ρ_{ZrO2} the density of the monoclinic zirconia (5.68 g cm^{-3}), M_{ZrO2} the molar mass of zirconia (123.2 g mol^{-1}) and n_{O_ZrO2} the amount of oxygen in the zirconia layer per unit area, expressed in mol m^{-2}. The corresponding oxygen amount per unit area for the three oxide thicknesses are summarized in Table 3.

$$n_{O\_Zr} = \frac{e_{ZrO_2}}{PBR} \times 10^{-9} \times 0.3 \times \frac{\rho_{Zr}}{M_{Zr}} \times 10^6 \tag{13}$$

with ρ_{Zr} the density of α-Zr (6.5 g cm^{-3}), M_{Zr} the atomic mass of zirconium and *PBR* the Pilling Bedworth ratio between zirconia and the alloy, taken at 1.56.

$$n_{O\_mobile} = n_{0\_ZrO_2} - n_{O\_Zr} \qquad (14)$$

The as-calculated theoretical amounts of oxygen per unit area inserted in the alloy (n_{O_mobile}) during the dissolution of a 70 nm, 340 nm and 670 nm-thick zirconia layer are presented in Table 3.

Table 3. Available oxygen amount per unit area (mol m^{-2}) and the residual oxygen quantities remaining in the metal in place of the oxide layer for 70 nm, 340 nm and 670 nm oxide thicknesses and the total dissolution temperature of these three oxide thicknesses obtained by FE simulation.

Oxide thickness (nm)	70	340	670
n_{O_ZrO2} (mol m^{-2})	0.00645	0.03135	0.06178
n_{O_Zr} (mol m^{-2})	0.00096	0.00467	0.00920
n_{O_mobile} (mol m^{-2})	0.00549	0.02668	0.05258
Temperature of total oxide dissolution obtained by FE calculations (K)	908	1023	1073

The FE calculations, using the experimental TDS temperature ramp as input data, give the temperatures at which the oxide layers are theoretically fully dissolved – under the hypothesis of uniform dissolution process – *i.e.* at which the corresponding "mobile" oxygen amount has crossed the oxide/metal interface. These temperatures, reported in Table 3, are compared to the experimental temperatures at which hydrogen desorption starts (second TDS peak), at which the hydrogen flux is maximal, and at which a heterogeneous oxide scale dissolution was observed by SEM, in figure 7.
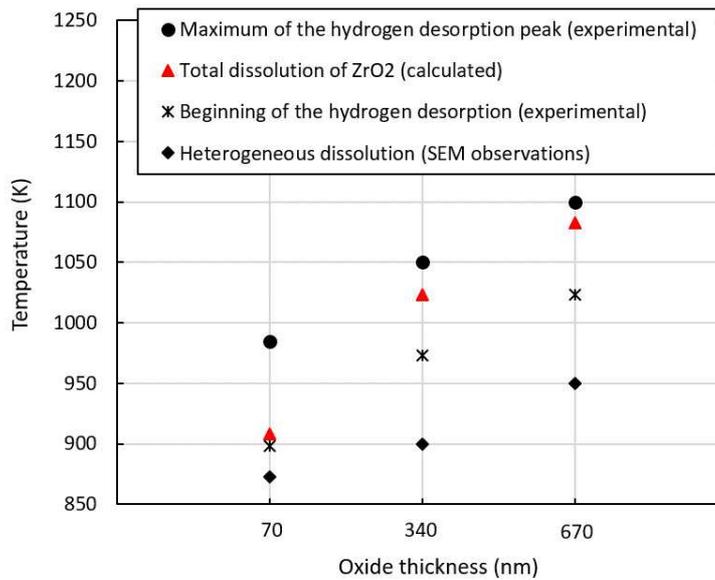
Fig. 7. Comparison between experimental temperatures for which hydrogen desorption starts (black crosses), for which hydrogen desorption flux is maximum in the TDS ramp (black circles), and for which heterogeneous dissolution was observed by SEM (black diamonds) with the theoretical total oxide dissolution temperature (red triangles), for the three oxide thicknesses on the specimens before the second TDS peak.

Figure 7 highlights systematically a hydrogen starting desorption temperature (black crosses) below the theoretical temperature for total dissolution of the oxide scales. This analysis is consistent with SEM observations (black diamonds), which showed that oxide dissolution was not uniform: the start of the second hydrogen TDS peak occurring sooner than the complete uniform dissolution may be explained by the presence of areas where the oxide scale is almost fully dissolved, from where hydrogen may be easily released.

Figure 7 also shows that the hydrogen maximum desorption temperature is systematically higher than the theoretical total oxide layer dissolution temperature, which indicates that, at least at the peak temperature, the system consists in hydrogen desorption from the metal without any oxide layer at its surface.

All these observations are in good agreement with a hydrogen desorption process that is kinetically controlled (or conditioned) by the dissolution of the oxide layer.

4.4   Challenging the hypothesis

In order to challenge our hypothesis that the zirconia oxide layer limits the hydrogen desorption during the temperature ramp, a last experiment was performed. Two Zy4 samples were oxidized: the first one at 673 K, the second one at 773 K in the thermogravimetric device in Ar-20%O_2 atmosphere

until a 340-nm and a 670-nm thick oxide layer were formed respectively. After oxidation, the specimens were submitted to two specific heat treatments in the TDS device that consisted in 5h at 873 K followed by 10h at 853 K for the 340-nm thick oxide specimen and 10h at 923 K followed by 8h at 873 K for 670-nm thick oxide sample. These specific heat treatments, aimed at completely dissolving the oxide layer, were identified according to a series of simulations based on Cast3M calculations using the approach detailed earlier. Once the layer dissolved, another TDS experiment was performed (without venting in the meantime) applying a 10 K min^{-1} temperature ramp from 293 K up to 1273 K to the specimen in order to observe the hydrogen desorption peak position and to measure the hydrogen amount remaining within the metal. Figure 8 compares the hydrogen thermal desorption thermograms obtained for specimens having undergone various conditions and heat treatments.
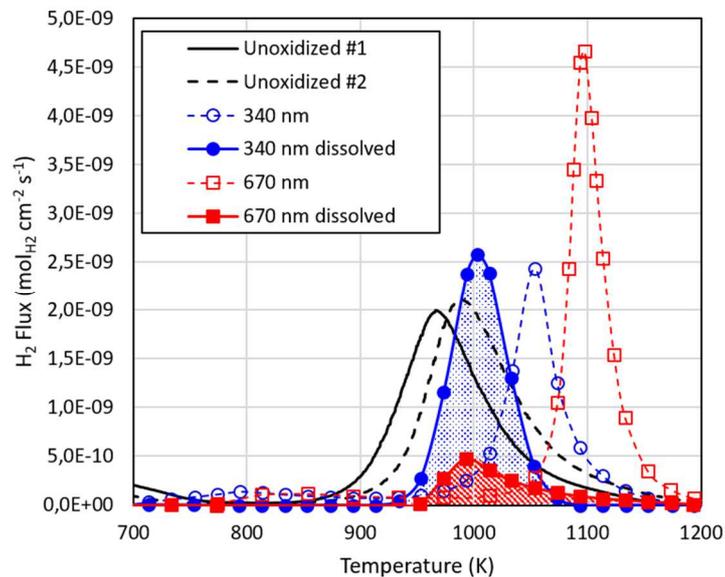

Fig. 8. Experimental TDS H$_2$ desorption fluxes (10 K min^{-1}) obtained on unoxidized Zy4 samples (black continuous and dashed curves), pre-oxidized Zy4 with 340 nm oxide thickness (blue empty circles), 670 nm oxide thickness (red empty squares), 340 nm oxide thickness dissolved (blue full circles) and 670 nm oxide thickness dissolved (red full squares).

After the oxide layer dissolution, the hydrogen desorption peak of the specimens shifted to lower temperatures (blue full circles and red full squares) whatever the initial oxide layer thickness. The hydrogen desorbed at close temperatures to those observed for the unoxidized Zy4 alloy (black continuous and dashed curves). After the dissolution of the 670-nm thick oxide, the hydrogen concentration remaining in the specimen (*i.e.* that desorbed during TDS, full red squares) was lower than before oxide dissolution (empty red squares). This lower desorbed hydrogen amount suggests that a part of the initial hydrogen amount had desorbed during the isothermal heat treatment.

These results demonstrate that, under vacuum, the hydrogen desorption from an oxide-covered Zy4 during a temperature ramp at 10 K min^{-1} is controlled by the oxide layer dissolution. We deduce that the hydrogen transport through the oxide is slower than the dissolution process during such temperature ramp. The oxide layer partially dissolves, which facilitates the hydrogen desorption from the alloy. Additional experiments would be needed to assess the rate-limiting step for hydrogen effusion in the case of a stable oxide layer covering the surface, *e.g.* during an isothermal treatment at medium-range temperature, and to thoroughly characterise the kinetic constants that are associated with this step. They will be the object of future works.

5   Conclusion

The effect of the presence of an oxide layer on the hydrogen desorption from Zircaloy-4 specimens was evaluated through thermogravimetric analyses and thermal desorption spectrometry. Zircaloy-4 samples were pre-oxidized to form different zirconia thicknesses on their surface, then hydrogen desorption in vacuum was monitored during a temperature ramp at 10 K min^{-1}. The results of these investigations, coupled to an oxide layer dissolution model implemented with the Cast3M code, are consistent with the following conclusions:

1. The oxide scale shifted the hydrogen desorption towards higher temperatures. It acted as a barrier to the hydrogen release from the alloy.
2. Hydrogen desorption started after partial dissolution of the oxide layer, when the oxide layer was still present in certain places and seemed to have completely disappeared from the surface of the metal elsewhere.
3. During such temperature ramp, the hydrogen transport through the oxide is slower than the oxide dissolution process.

The rate-limiting step of the hydrogen desorption process during isothermal treatments at lower temperature without – or with limited – oxide dissolution will be studied in future works.

6   Data availability

The raw/processed data required to reproduce these findings cannot be shared at this time as the data also forms part of an ongoing study.

7 Acknowledgements

8 References

[1]   IAEA, Waterside corrosion of zirconium alloys in nuclear power plants, Int. At. Energy Agency. TECDOC-996 (1998).

[2]   C. Juillet, M. Tupin, F. Martin, Q. Auzoux, C. Berthinier, F. Miserque, F. Gaudier, Kinetics of hydrogen desorption from Zircaloy-4: Experimental and modelling, Int. J. Hydrog. Energy. 44 (2019) 21264–21278.

[3]   M. Wilde, K. Fukutani, Penetration mechanisms of surface-adsorbed hydrogen atoms into bulk metals: Experiment and model, Phys. Rev. B. 78 (2008).

[4]   M. Martin, C. Gommel, C. Borkhart, E. Fromm, Absorption and desorption kinetics of hydrogen storage alloys, J. Alloys Compd. 238 (1996) 193–201.

[5]   M.W. Mallet, W.M. Albrecht, Low-Pressure Solubility and Diffusion of Hydrogen in Zirconium, J. Electrochem. Soc. 104 (1957) 142.

[6]   G. Amsel, D. David, G. Beranger, P. Boisot, B. De Gelas, P. Lacombe, Analyse a l'aide d'une methode nucleaire des impuretes introduites dans les metaux par leurs preparations d'etat de surface: Application au zirconium, J. Nucl. Mater. 29 (1969) 144–153.

[7]   C.R. Cupp, P. Flubacher, An autoradiographic technique for the study of tritium in metals and its application to diffusion in zirconium at 149° to 240° C, J. Nucl. Mater. 6 (1962) 213–228.

[8]   G.U. Greger, H. Münzel, W. Kunz, A. Schwierczinski, Diffusion of tritium in zircaloy-2, J. Nucl. Mater. 88 (1980) 15–22.

[9]   A. Sawatzky, The diffusion and solubility of hydrogen in the alpha phase of Zircaloy-2, J. Nucl. Mater. 2 (1960) 62–68.

[10] C. Schwartz, M. Mallet, Observation of the behavior of hydrogen in zirconium, Trans. Am. Soc. Met. 46 (1954) 641–654.

[11] B.F. Kammenzind, D.G. Franklin, H.R. Peters, W.J. Duffin, Hydrogen Pickup and redristribution in alpha annealed Zircaloy-4, Zircon. Nucl. Ind. 11th Int. Symp. ASTM STP 1295. (1996) 338.

[12] C.-S. Zhang, B. Li, P.R. Norton, The study of hydrogen segregation on Zr(0001) and Zr(1010) surfaces by static secondary ion mass spectroscopy, work function, Auger electron spectroscopy and nuclear reaction analysis, J. Alloys Compd. 231 (1995) 354–363.

[13] J.H. Austin, T.S. Elleman, K. Verghese, Tritium diffusion in zircaloy-2 in the temperature range −78 to 204° C, J. Nucl. Mater. 51 (1974) 321–329.

[14] M. Tupin, F. Martin, C. Bisor, R. Verlet, P. Bossis, J. Chene, F. Jomard, P. Berger, S. Pascal, N. Nuns, Hydrogen diffusion process in the oxides formed on zirconium alloys during corrosion in pressurized water reactor conditions, Corros. Sci. 116 (2017) 1–13.

[15] I. Takagi, K. Une, S. Miyamura, T. Kobayashi, Deuterium diffusion in steam-corroded oxide layer of zirconium alloys, J. Nucl. Mater. 419 (2011) 339–346.

[16] W. Kunz, H. Münzel, U. Kunz, Tritium release from Zircaloy-2: Dependence on temperature, surface conditions and composition of surrounding medium, J. Nucl. Mater. 136 (1985) 6–15.

[17] C. Andrieu, Etude de la permeation du tritium à travers les gaines de crayons combustibles type REP, Université de Grenoble, 1998.

[18] W. Chen, L. Wang, S. Lu, Influence of oxide layer on hydrogen desorption from zirconium hydride, J. Alloys Compd. 469 (2009) 142–145.

[19] W. Kunz, H. Münzel, U. Helfrich, Diffusion of tritium in zircaloy: Influence of low irradiation damage, oxygen concentration and formation of δ-hydrides, J. Nucl. Mater. 105 (1982) 178–183.

[20] D. Wongsawaeng, S. Jaiyen, High-temperature absolute hydrogen desorption kinetics of zirconium hydride under clean and oxidized surface conditions, J. Nucl. Mater. 403 (2010) 19–24.

[21] A. Roustila, J. Chêne, C. Séverac, XPS study of hydrogen and oxygen interactions on the surface of zirconium, J. Alloys Compd. 356–357 (2003) 330–335.

[22] C. Andrieu, S. Ravel, G. Ducros, C. Lemaignan, Release of fission tritium through Zircaloy-4 fuel cladding tubes, J. Nucl. Mater. 347 (2005) 12–19.

[23] X. Ma, C. Toffolon-Masclet, T. Guilbert, D. Hamon, J.C. Brachet, Oxidation kinetics and oxygen diffusion in low-tin Zircaloy-4 up to 1523K, J. Nucl. Mater. 377 (2008) 359–369.

[24] J.P. Abriata, J. Garcés, R. Versaci, The O–Zr (Oxygen-Zirconium) system, Bull. Alloy Phase Diagr. 7 (1986) 116–124.

[25] Y. Hirohata, T. Nakamura, Y. Aihara, T. Hino, Dependence of surface oxidation on hydrogen absorption and desorption behaviors of Ti–6Al–4V alloy, J. Nucl. Mater. 266 (1999) 831–836.

[26] I.S. Dupim, J.M.L. Moreira, J. Huot, S.F. Santos, Effect of cold rolling on the hydrogen absorption and desorption kinetics of Zircaloy-4, Mater. Chem. Phys. 155 (2015) 241–245.

[27] J. Sayers, S. Ortner, S. Lozano-Perez, Effect of pH on hydrogen pick-up and corrosion in zircaloy-4, Miner. Met. Mater. Ser. Part F9 (2018) 1169–1180.

[28] www-cast3m.cea.fr/

[29] G. Zumpicchiat, S. Pascal, M. Tupin, C. Berdin-Méric, Finite element modelling of the oxidation kinetics of Zircaloy-4 with a controlled metal-oxide interface and the influence of growth stress, Corros. Sci. 100 (2015) 209–221.

[30] M. Tupin, M. Pijolat, F. Valdivieso, M. Soustelle, A. Frichet, P. Barberis, Differences in reactivity of oxide growth during the oxidation of Zircaloy-4 in water vapour before and after the kinetic transition, J. Nucl. Mater. 317 (2003) 130–144.

[31] U.R. Evans, The relation between tarnishing and corrosion, Trans Electrochem Soc. 46 (1924) 247.

[32] P. Barret, Cinetique heterogene., Gauthier-Villars, Paris, 1973.

[33] M. Parise, Mécanismes de corrosion des alliages de zirconium : étude des cinétiques initiales d'oxydation et du comportement mécanique du système métal – oxyde, Ecole Nationale Supérieure des Mines de Paris, 1996.

[34] B. Cox, C. Roy, Transport of Oxygen in Oxide Films on Zirconium Determined by the Nuclear Reaction O17 (He3,a)O16, Electrochem. Technol. 4 (1966) 121.

[35] D. Douglass, Corrosion of reactor materials, IAEA Proc. (1962).

[36] J. Debuigne, P. Lehr, The determination of oxygen diffusion coefficient in the Zirconium-Oxygen system, IAEA Proc. (1962).